https://doi.org/10.20965/jrm.2011.p0105

Paper:

Active Catheters for Neuroradiology

Jérôme Szewczyk[*1], **Emilie Marchandise**[*2], **Patrice Flaud**[*3], **Laurent Royon**[*3], **and Raphaël Blanc**[*4]

[*1]Institut des Systèmes Intelligents et de Robotique, Université Pierre et Marie Curie (Paris VI), France
[*2]Institute of Mechanics, Materials and Civil Engineering, Université Catholique de Louvain (UCL), Belgium
[*3]Laboratoire Matière et Systèmes Complexes CNRS, Université Paris Diderot, France
[*4]Service de Radiologie, Fondation Rothschild Hospital, Paris, France
E-mail: jerome.szewczyk@isir.fr
[Received April 21, 2010; accepted July 29, 2010]

Surgeons performing endovascular interventions have high expectations with regard to the improvement of their operating tools and, more specifically, of their catheters. Active catheters, in which the tip moves actively using Shape Memory Alloy (SMA) actuators, constitute a promising approach. In this article, we review existing SMA-based active catheters present in the literature. We analyze their performances regarding the requirements imparted to neuroradiology. Then, we propose a new analytical model for predicting the thermo-mechanical behavior of steerable catheters actuated through SMA wires. Particularly, we give an expression for the maximal achievable bending angle of the catheter tip. These results are finally applied to the design of single-use small-diameter active catheters especially devoted to neuroradiology. In particular, we present a 3.3-Fr catheter suited for navigating into the Willis' polygon and for accurate positioning into aneurysmal cavities.

Keywords: active catheter, SMA actuator, neuroradiology

1. Introduction

Surgeons performing endovascular surgery (interventional cardiology or neuroradiology, etc.) have high expectations with regard to the improvement of their operating tools and, more specifically, of their catheters. Because of their length and great flexibility, these devices appear to be significantly limited with respect to commandability, precision, and stability. In neuroradiology, in particular, the route through which the catheter must travel from the insertion point (commonly the femoral artery at the groin) to the pathology area (e.g., a cerebral aneurysm) often involves very small vessels with tight radii and large branching angles. Furthermore, neuroradiologists still encounter difficulties in accurately positioning the catheter at the center of the aneurysmal cavity for coil insertion (see **Fig. 1**).

Various solutions having the form of drivable active catheters were proposed in the literature. For example, Guo et al. [1] imagined a micro-actuator based on the Ionic Conductive Polymer Film (ICPF) technology for controlling the bending of a catheter tip. In Ref. [2], the electrochemical actuation of a catheter coated with polypyrrole is studied. Ikuta et al. [3] produced a hydrodynamic active catheter driven by integrated micro valves. Shape Memory Alloy (SMA) actuators were also widely investigated. SMA actuators present a number of advantages when applied to active catheterism. They are biocompatible and have an excellent density-to-power ratio [4, 5]. The concept of SMA actuation for catheterism is depicted in **Fig. 2**. The bending motion is obtained by an electrical current i which generates heat by the Joule effect, which induces a phase transformation of the SMA actuator. More than one SMA actuator are generally integrated at the tip of the catheter in order to fully control its bending in the 3-D space. The cross section of a catheter featured with three SMA actuators disposed at 120° from each other is depicted in **Fig. 3**.

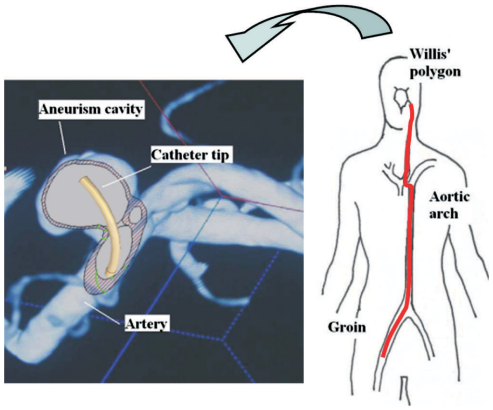

Fig. 1. Route of the catheter in the arterial frame.

Wire-shaped SMA actuators were primarily exploited in the design of active catheters for their simplicity and their high stress capability. For example, Fukuda et al. [6] and Takizawa et al. [7] have developed catheters with external diameters of about 1.5 mm and actuated by three SMA wires distributed at interval of 120° around the

Table 1. Performances of active catheters found in the literature.

Authors	Ref	External diameter (mm)	Shape	Number of actuators	Bending angle per unit (deg)	Length of the unit (mm)	Radius of curvature (mm)
Fukuda	[6]	1.65	Wire	3	32	15	27
Mizuno	[8]	2.6	Wire	2	90	20	12.7
Takizawa	[7]	1.5	Wire	3	> 45	20	25.5
Mineta	[15]	0.9	Flat spring	3	14	3.1	12.7
Chang	[14]	3.0	Flat spring	3	90	40	25.5
Fu	[10]	1.3	Coil	3	90	92	59
Haga	[11]	1.6	Coil	3	45	19	24.2
Lim	[12]	2.8	Coil	3	13	3	55
Park	[13]	2.0	Coil	3	50	5	5.7

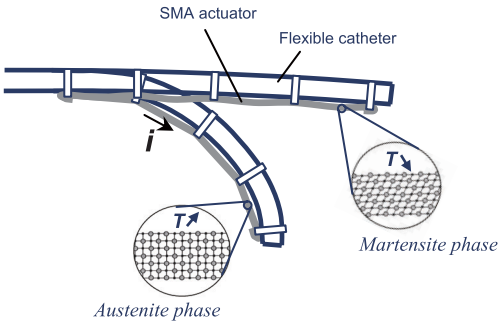

Fig. 2. SMA actuated catheter (principle).

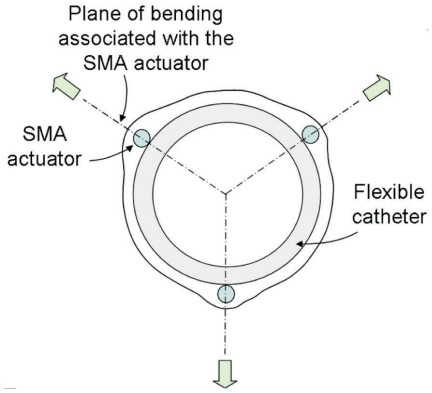

Fig. 3. Active catheter featured with three SMA actuators.

catheter. In Ref. [8], a similar device with a diameter of 2.6 mm has been applied to peroral pancreatoscopy in pigs. In Ref. [9], the principle of a catheter having a spiral structure made of a flexible belt integrating SMA wires is presented.

Coil-shaped SMA micro-actuators were also used for their high strain capability [10]. In Ref. [11], the fabrication of a 1.4-mm-diameter catheter using SMA coils as actuators with bending, torsional, and extending control capabilities is detailed. A multi-link active catheter which fabrication is based on silicon micromachining is presented in Ref. [12], together with an interesting method for the indirect heating of the SMA coils. In Ref. [13], a multi-link active catheter including a polyimide-based integrated CMOS interface circuit for communication and control is presented.

SMA actuators having the shape of flat springs have also been used regarding the possibility to produce very small actuators [14]. In Ref. [15], a 0.9-mm-diameter catheter has been realized this way. More recently, Kubo et al. [16] and Langelaar and Van Keulen [17] studied the feasibility of active catheters cut from thin SMA tubes. **Table 1** summarizes the main characteristics of active catheters with small diameters that have been presented and evaluated in the literature.

To our knowledge, none of these devices entirely satisfy the constraints imposed by neuroradiology. Applying the concept of active catheterism to neuroradiology indeed raises particular requirements:

(1) Technological complexity and high cost of realization are prohibited with respect to the principle of single-use device.

(2) Diameters close to the millimeter are mandatory because of the thickness of brain arteries.

(3) Most of the time, placing the catheter tip at the center of aneurysm cavities requires radii of curvature to be smaller than 10 mm [18].

As we can see in **Table 1**, the prototype of Mineta [15] is the only one that simultaneously satisfies the two constraints relative to the diameter and to the radius of curvature. This prototype is shown in **Fig. 4**. It integrates batch-fabricated small flat NiTi springs as actuators and a three-dimensional super-elastic helicoidal coil as bias spring obtained by photolithography and electrochemical etching. This realization process is complex and poorly compatible with the low-cost constraint.

In this article, we present a new approach for the design of simple, low-cost, and very small active catheters suited for neuroradiology. Our method is based on a deep understanding of the theoretical behavior of active catheters and the experimental validation of several prototypes. The structure of the article is divided into three

Table 2. Notations.

σ	radial stress applied by a SMA wire	$\lambda_{\max}$	length of the bendable portion of catheter
T	axial force applied by a SMA wire	$\theta(\lambda)$	bending angle along the neutral axis
r	distance from SMA to the neutral axis	$\theta_{\max}$	total bending angle of the catheter
d	diameter of the SMA wire	$\tilde{\theta}_{\max}$	measured value of the total bending angle
E_A	SMA Young modulus in austenite state	$\tau_{\min}$	strain rate starting the martensite plateau
E_M	SMA Young modulus in martensite state	$\tau_{\max}$	strain rate ending the martensite plateau
E_C	Young modulus of the catheter structure	τ_{init}	rate of pre-strain
λ	local coordinate along the neutral axis	$\hat{\tau}_{init}$	optimal rate of pre-strain

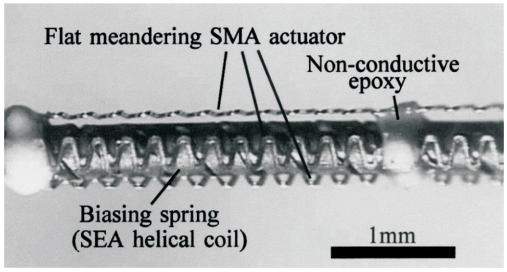

Fig. 4. The active catheter of Mineta [15].

parts: (i) first, we present and validate a new kinemato-static behavior model for active catheters featured with SMA wire actuators. (ii) Simple conceptual rules useful for the optimal design of active catheters are derived from this model and two active catheters having the required characteristics for neuroradiological applications are realized. (iii) The performances of these two prototypes are qualitatively evidenced through in-vitro experiments emulating navigation in arteries and embolization of small cerebral aneurysms.

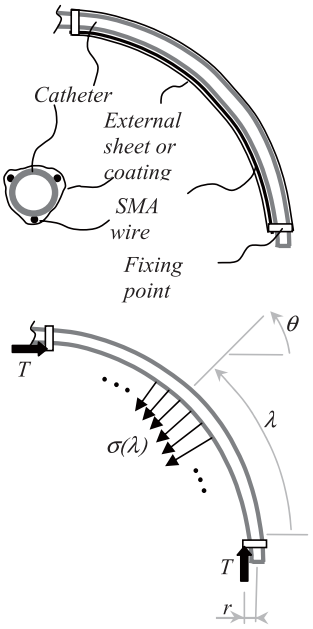

Fig. 5. Interaction between an SMA wire and the catheter structure.

2. Mechanical Behavior of SMA-Based Active Catheters

The following kinemato-static model of an active catheter aims to establish the mathematical relations existing between its physical parameters and its main mechanical performances. For clarity purposes, we will focus on the maximal bending angle the catheter can achieve. **Table 2** summarizes our notations.

In Ref. [13], the mechanical behavior of an active catheter featured with SMA micro-coils is analyzed relying on the circular bending assumption. In Ref. [10], a more precise model, independent from this assumption, is presented. However, in this model, SMA actuators do not bend with the catheter structure but remain linearly stretched between their fixing points. In Ref. [6], Fukuda et al. address the more realistic case of SMA actuators that always follow the curvature of the catheter. However, the derived expression for the maximal bending angle of the device is not independent from the unknown stress that the SMA wires undergo.

In this section, we give a reliable model for the SMA-based active catheter depicted in **Fig. 5**. It is featured with three wire-shaped SMA actuators having the stress-strain characteristics of **Fig. 6**. In this figure, we also qualitatively indicate the functioning point of each SMA wire in the stress-strain plane when the catheter is at rest and when it is bended.

The mechanical load applied by an SMA wire (either activated or not) to the structure has two components: (1) a compression force T applied at the two fixing points, and (2) a shear stress σ distributed along the structure between the two fixing points and located into the bending plane (see **Fig. 5**).

The shear stress $\sigma(\lambda)$ applied by an SMA wire (either activated or not) to the catheter uniquely depends on the axial force T it produces and on the local curvature of the structure:

$$\sigma(\lambda) = T \cdot \frac{\partial \theta(\lambda)}{\partial \lambda} \quad \ldots\ldots\ldots\ldots \quad (1)$$

where λ and θ are respectively the curvilinear coordinate and the bending angle at a specific point of the neutral axis.

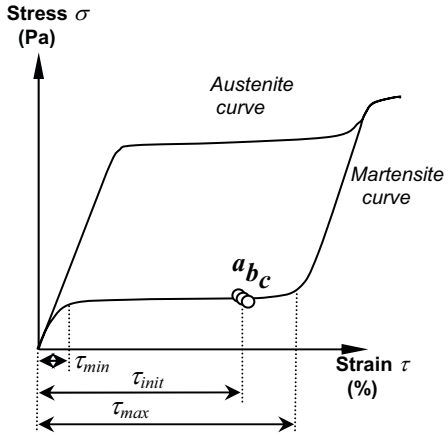

A- Functionning points of the three SMA actuators (*a,b,c*) when the catheter is straight and at rest

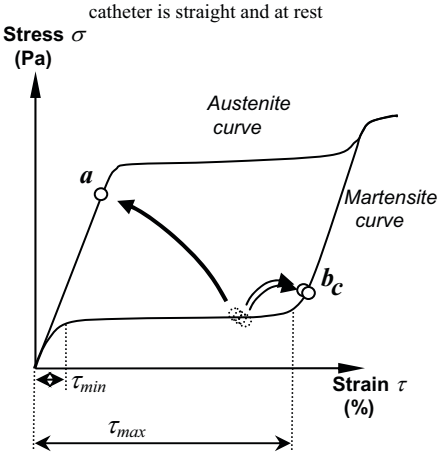

B- Functionning points of the three SMA actuators when the catheter is bended (a : activated wire, b & c : passive wires)

Fig. 6. Thermo-mechanical behavior of the SMA actuators.

In the following, it is assumed that among the three SMA wires, only one is activated and fully austenite transformed while the two others remain in their martensite state and resist to the flexion. Using Eq. (1), one can also demonstrate (see Appendix A) that the bending moment applied by an SMA wire is constant along the structure and proportional to the difference between the force T_A applied by the activated wire and the force T_M applied by one passive wire:

$$M = r \cdot (T_A - T_M) \quad . \quad . \quad . \quad . \quad . \quad . \quad . \quad . \quad . \quad . \quad . \quad (2)$$

Assuming that the catheter material is homogenous, this implies that the curvature $\frac{\partial \theta(\lambda)}{\partial \lambda}$ is constant and that the shape of the bended catheter is circular.

Using Eq. (2) in the context of large deflexions, one can derive an expression for the maximal bending angle $\theta_{\max}$ a catheter featured with three SMA wires can reach. The expression of $\theta_{\max}$ depends on the pre-strain τ_{init} identically imposed to the three SMA wires during the assembly process. Assuming that the distance r is close to the catheter radius, it can be seen that (see Appendix B):

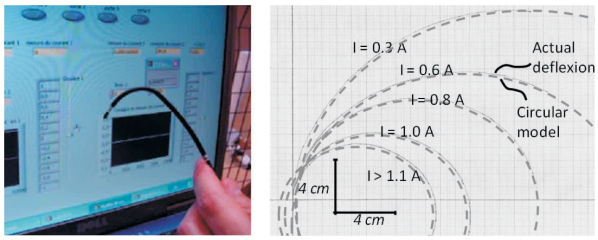

Fig. 7. Experimental validation of the model.

If $\tau_{init} \leq \hat{\tau}_{init}$ then:

$$\theta_{\max} \approx \frac{\lambda_{\max}}{r}\left(\tau_{init} - \frac{E_M}{E_A}\tau_{\min}\right)\left(1 + \tau_{init} + \frac{r^2 E_C}{d^2 E_A}\right)^{-1} \quad (3)$$

If $\tau_{init} > \hat{\tau}_{init}$ then

$$\theta_{\max} \approx \frac{\lambda_{\max}}{r}\left(\tau_{\max} - \frac{E_M}{E_A}\tau_{\min}\right)\left(\frac{3}{2}(1 + \tau_{init}) + \frac{r^2 E_C}{d^2 E_A}\right)^{-1} \quad . \quad . \quad . \quad . \quad . \quad . \quad . \quad . \quad . \quad . \quad . \quad . \quad . \quad . \quad . \quad . \quad . \quad (4)$$

Here, $\hat{\tau}_{init}$ is the largest rate of pre-strain τ_{init} that permits to keep the functioning point of the two stretched passive SMA wires on the martensite plateau during the catheter flexion (i.e., their strain τ remains lower than $\tau_{\max}$ (see **Fig. 6**)). One can see (see Appendix C) that $\hat{\tau}_{init}$ also constitutes an optimal choice for τ_{init} that maximizes the angle $\theta_{\max}$. A close approximation for $\hat{\tau}_{init}$ is:

$$\hat{\tau}_{init} \approx \frac{K+1}{K+1.5}\tau_{\max} \text{ with } K = \frac{r^2 E_C}{d^2 E_A} \quad . \quad . \quad . \quad . \quad (5)$$

Note that Eqs. (3) and (4) have been derived assuming that the activated SMA wire in its complete austenite state undergoes an internal stress that remains under the superelasticity threshold of the material.

Equations (2) and (3) were experimentally validated by assessing the bending shape and magnitude of the prototype shown in **Fig. 7**. Its geometrical and physical parameters are presented in **Table 3**. In this table, we have also reported the theoretical expected value of $\theta_{\max}$ and its maximal uncertainty deduced from the uncertainties on the model parameters. Note that the prototype is featured with a unique SMA actuator. For this reason, we set the parameter E_M to zero in the above expression of $\theta_{\max}$ (no passive SMA wire).

We powered this first prototype with an electrical current whose intensity varied from 0 to more than 1.1 A. In **Fig. 7**, we have reported the successive bending configurations reached by the catheter for five different current intensities. As we can see, all these configurations are very close to perfect circles as predicted by our model. The maximal bending angle for this prototype was found to be $\tilde{\theta}_{\max} = 3.90 \pm 0.20$ rad. On the other hand, Eqs. (3) and (5) lead to $\theta_{\max} = 3.51 \pm 0.76$ rad.

Table 3. Characteristics of the first prototype.

	r (mm)	D (mm)	E_A (GPa)	E_M (GPa)	E_C (GPa)	$\lambda_{\max}$ (mm)	$\tau_{\min}$	$\tau_{\max}$	τ_{init}	$\theta_{\max}$ (rad)
Nominal values	1.2	0.25	30	0	0.9	158	0.015	0.06	0.046	**3.509**
Uncertainties	0.02	0.005	2	0	0.05	2	0.005	0.005	0.005	**0.756**

3. Two Active Catheters Specially Designed for Neuroradiology

Regarding Eq. (5), it appears that the bending angle $\theta_{\max}$ can be maximized by observing some simple designing rules. Indeed, for a catheter structure with a given size and material, one should:

- Minimize r (i.e., the embedded SMA actuators should lie as close as possible to the neutral axis of the catheter).
- Choose an SMA material that maximizes the parameters $\tau_{\max}$ and E_A.
- Choose the SMA wires' diameter d to be as large as possible, taking into account the limit imposed to the device external diameter.
- Pre-strain the SMA wires with a rate close to $\hat{\tau}_{init}$.

Eq. (5) also implies that:

- Applying a scale factor $\alpha < 1$ to r, d and $\lambda_{\max}$ will result in a decrease of the catheter radius of curvature by the same scale factor but will conserve the maximal bending angle $\theta_{\max}$.
- Applying a scale factor $\alpha < 1$ only to r and d will conserve the radius of curvature but will result in an increase of $\theta_{\max}$ by a factor $1/\alpha$.

These recommendations and considerations were applied to the production of two active catheters. The first one is a 2.0-mm external diameter catheter with an internal lumen of 1.4 mm (**Fig. 8(a)**). It emulates a 6-Fr standard guiding catheter useful for navigating from the insertion point to the carotid artery. Its dimensions are compatible with the use of a standard introductor and guide wire. The second one is an ultra-fine catheter having an external diameter of 1.2 mm and an internal lumen of 0.5 mm. It emulates a 3.3-Fr standard micro-catheter suited for the navigation in the tiny brain arteries and the positioning into aneurysmal cavities. The assembly process for both prototypes (**Fig. 8**) relies on the cramping method described in the French patent application [19]. It does not require any soldering nor complex electrical connexion and enables to perfectly align the SMA wires fixing points and beads with the catheter axis. The beads keep the SMA wires attached to the catheter's surface during the flexion. The distances between two consecutive beads for both prototypes were chosen empirically. Insulation can be obtained by covering the distal part of the catheter with a thin sheath of silicone elastomer like the Silibione^{TM} for example. The SMA wires are 50-μm and 100-μm cold worked, straight annealed NiTi wires made by the Memory$^{®}$GMBH company (http://www.memory-metalle.de).

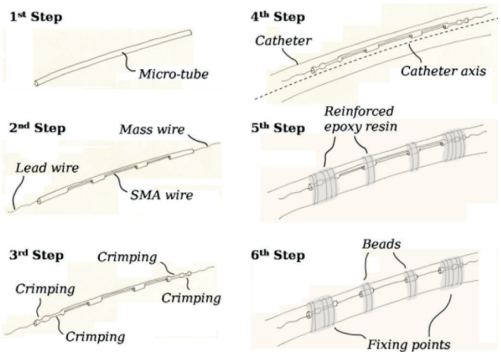

(a)

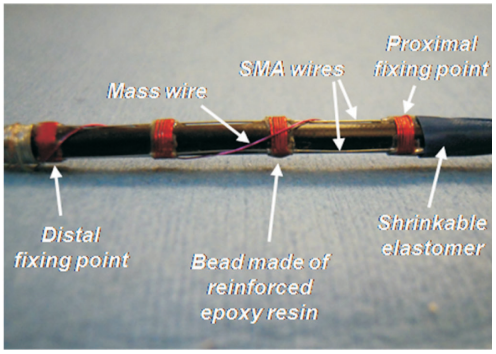

(b)

Fig. 8. Details of the assembly and partial view of a 6-Fr active catheter (before overcoating).

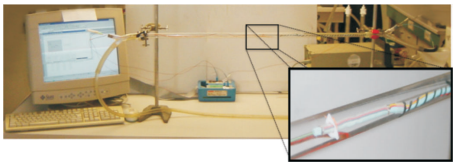

Fig. 9. Experimental set-up for temperature assessment.

4. Experimental Validation of the Prototypes

First, the thermal biocompatibility of these devices was verified using the set up shown in **Fig. 9**. This experimental device consists of a hydrodynamic loop where the catheter is placed inside a linear straight test section and is and fixed to its ends to remain straight. The water temperature is maintained at 37°C and the water mean velocity

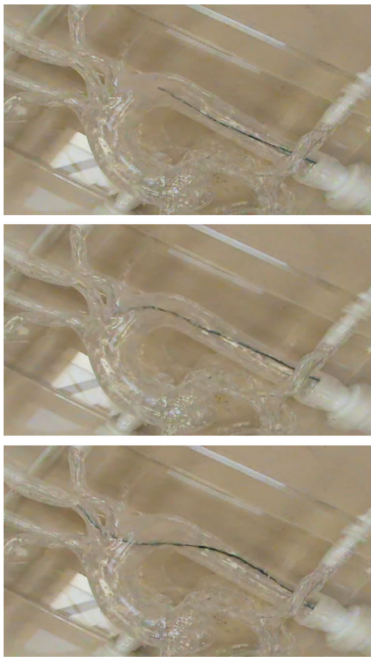

Fig. 10. 6-Fr prototype going through the aortic arch.

is taken to be 20 cm/s, as this value is close to blood flow velocity in the aorta. The SMA wires are then connected to a generator which can deliver a constant current in the range 500 mA to 2000 mA. In order to measure the surface temperature of the catheter, a Cu-constantan T-type thermocouple wire of 700 μm diameter is glued onto the outer surface of polyester film just above the SMA wire. Results show that the surface temperature never exceeds 41°C for a constant current intensity up to 2 A. More details on this thermal characterization can be found in Ref. [20].

Then, the performances of the two prototypes were qualitatively evaluated using two realistic 3-D and 2-D anatomical models. **Fig. 10** shows how the 6-Fr (2 mm) prototype allows passage through the aortic arch and entrance to the carotid artery. This task was performed without difficulties by a non-initiated operator.

Figure 11 shows the 3.3-Fr (1.2 mm) prototype progressing into the fine arteries of the Willis' polygon. This experiment shows how SMA actuators can also be used to precisely place the catheter distal extremity at the center of cerebral aneurysms (see 2nd and 4th pictures of **Fig. 11**). As depicted in **Fig. 11** (4th picture), its maximal bending angle is greater than 70° and its minimal radius of curvature is about 9 mm.

Note also that these two prototypes have sufficient bending rate regarding the targeted medical application. For example, the second prototype can bend to 70° in less than 2 s.

5. Conclusion

Drivable catheters actuated through shape memory alloy are a promising approach for the endovascular treatment of pathologic conditions involving cervical and intracranial vessels. In this article, we have evaluated this concept both analytically and experimentally.

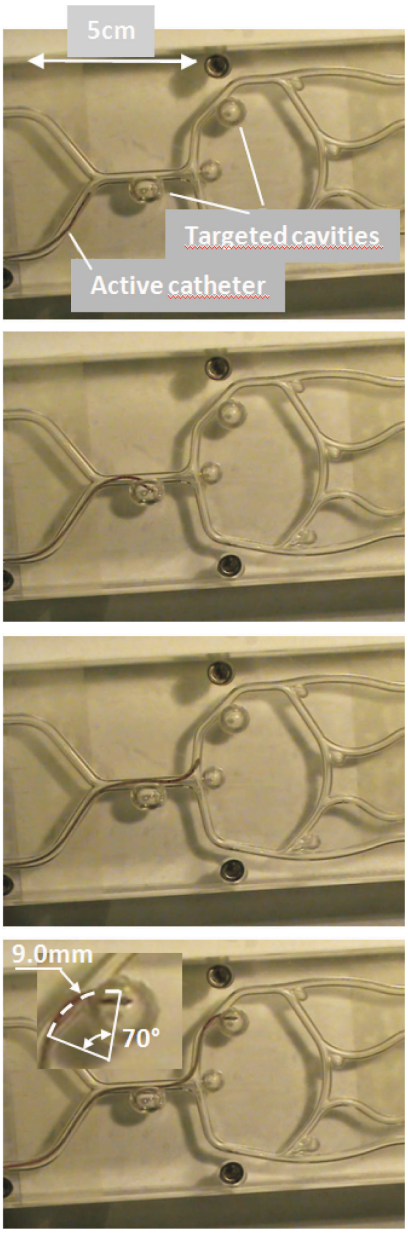

Fig. 11. 3.3Fr catheter navigating through the Willis'polygon.

An original kinemato-static model for this kind of device has been presented and tested. It relies on a realistic description of:

1. The mechanical interaction between the SMA wires and the catheter structure.
2. The thermo-mechanical behavior of the NiTi material.

Two different prototypes of active catheters were designed based on information derived from the proposed model. They were experimented on realistic anatomical phantoms. Particularly, a 1.2-mm-diameter catheter actuated by SMA wires was realized and proved to be suited

for distal extremity controlling and positioning.

In future works, in-vivo evaluations of our prototypes will be conducted in pig and rabbit. Additionally, we will improve our design approach by considering other criteria such as energy consumption and dynamical behavior. For this purpose, a fluid-thermal simulation program describing active catheters evolving in blood is currently under development [20]. Besides, the control issue will be addressed. To this purpose, a new scheme specially devoted to position control of antagonist SMA actuators has been proposed in [21] and tested within the framework of endoscopic applications. At the supervision level, we are currently studying the possibility to combine pre-acquired CT angiography and in-line catheter pose reconstruction to provide a 3D road mapping for active catheters [22].

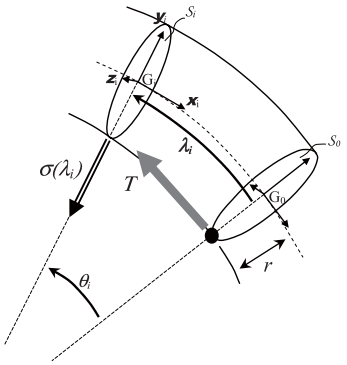

Fig. 12. Mechanical interaction between the catheter and the SMA wire.

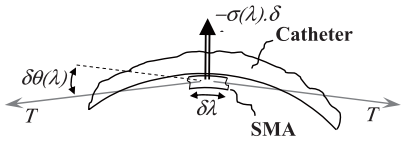

Fig. 13. Static equilibrium at any point of the SMA wire.

References:

[1] S. Guo et al., "Micro Catheter System with Active Guide Wire," IEEE Int. Conf. on Robotics and Automation, pp. 79-84, 1995.

[2] T. Shoa et al., "Conducting Polymer Based Active Catheter for Minimally Invasive Interventions inside Arteries," IEEE Int. Conf. of the Eng. in Medicine and Biology Society, pp. 2063-2066, 2008.

[3] K. Ikuta et al., "Hydrodynamic Active Catheter with Multi Degrees of Freedom Motion," IFMBE World Congress on Medical Physics and Biomedical Engineering, pp. 3091-3094, 2007.

[4] S. Shabalovskaya, "On the nature of the biocompatibility and on medical applications of niti shape memory and superelastic alloys," Biomed Mater Eng, Vol.6, No.4, pp. 267-289, 1996.

[5] J. Peirs, D. Reynaerts, and H. Van Brussel, "The true power of SMA micro-actuation," MicroMechanics Europe Workshop, pp. 217-220, 2001.

[6] T. Fukuda, S. Guo, K. Kosuge, F. Arai, M. Negoro, and K. Nakabayashi, "Micro active catheter system with multi degrees of freedom," IEEE Int. Conf. on Robotics and Automation, pp. 2290-2295, 1994.

[7] H. Takizawa, H. Tosaka, R. Ohta, S. Kaneko, and Y. Ueda, "Development of a Micro fine active bending catheter equipped with mif tactile sensors," IEEE Int. Conf. on Micro Electro Mechanical Systems, pp. 412-417, 1998.

[8] S. Mizuno et al., "Shape memory alloy catheter system for peroral pancreatoscopy using an ultrathin-caliber endoscope," Endoscopy, Vol.26, No.8, pp. 676-680, 1994.

[9] Y. Koseki et al., "Development of a Spiral Structure for an Active Catheter Overview of the Spiral Structure and Its Kinematic Configuration," IEEE/RSJ Int. Conf. on Intelligent Robots and Systems, Vol.2, pp. 1259-1264, 1999.

[10] Y. Fu et al., "Research on the axis shape of an active catheter," Int. J. of Medical Robotics and Computer Assisted Surgery, Vol.4, pp. 69-76, 2008.

[11] Y. Haga, Y. Tanahashi, and M. Esashi, "Small diameter active catheter using shape memory alloy," IEEE Int. Conf. on Micro Electro Mechanical Systems, pp. 419-424, 1998.

[12] G. Lim et al., "Active catheter with multi-link structure based on silicon micromachining," IEEE Int. Conf. on Micro Electro Mechanical Systems, pp. 116-121, 1995.

[13] K. Park and M. Esashi, "A multilink active catheter with polyamide-based integrated CMOS interface circuit," J. of Microelectromechanical Systems, Vol.8, No.4, pp. 349-356, 1996.

[14] J. Chang, S. Chung, Y. Lee, and J. Park, "Development of endovascular microtools," J. of Micromechanics and Micro-engineering, Vol.12, pp. 824-831, 2002.

[15] T. Mineta, T. Mitsui, Y. Watanabe, S. Kobayashi, Y. Haga, and M. Esashi, "Batch fabricated flat meandering shape memory alloy actuator for active catheter," Sensors and Actuators A, Vol.88, pp. 112-120, 2001.

[16] H. Kubo et al., "Fabrication of Microactuator for Active Catheter from SMA Thin Film Tube," 21st Sensor Symposium on Sensors, Micromachines and Applied Systems, pp. 39-42, 2004.

[17] M. Langelaar and F. Van Keulen, "Design optimization of shape memory alloy active structures using the R-phase transformation," SPIE Conf. on Active and Passive Smart Structures and Integrated Systems, pp. 6525-6530, 2007.

[18] T. Abe, "Distal-Tip Shape-Consistency Testing of Steam-Shaped Microcatheters Suitable for Cerebral Aneurysm Coil Placement," J. of Neuroradiology, Vol.25, pp. 1058-1061, June/July 2004.

[19] J. Szewczyk, "Méthode pour assemblage des cathéters / Méthode d'amélioration des courbures des cathéters et autres," French patent application FR, 10, 52119, 2010.

[20] E. Marchandise, L. Royon, P. Flaud, J. Szewczyk, and R. Blanc, "Thermal and hydrodynamic modeling of active catheters for the neuroradiology," Computer Methods in Biomechanics and Biomedical Engineering, 2010.

[21] V. DeSars, S. Haliyo, and J. Szewczyk, "A Practical Approach to the Design and Control of Active Endoscopes," Mechatronics, Vol.20, No.2, pp. 251-264, 2010.

[22] C.-J. Lin, R. Blanc, F. Clarençon, M. Piotin, L. Spelle, J. Guillermic, and J. Moret, "Overlying Fluoroscopy and Preacquired CT Angiography for Road-Mapping in Cerebral Angiography," AJNR American J. of Neuroradiology, Vol.31, technical note, March 2010.

Appendix A.

We first consider a catheter featured with only one SMA wire. As depicted in **Fig. 12**, this wire applies to the structure an axial tip force $T = -T\mathbf{x}_0$ and a distributed shear stress $\sigma(\lambda) = -\sigma(\lambda)\mathbf{y}_\lambda$ all along the line it is connected to the catheter. **Fig. 13** illustrates the local relation between the stress $\sigma(\lambda)$, the curvature of the catheter $\frac{\partial\theta(\lambda)}{\partial\lambda}$ and the axial force T. As we can see, the static equilibrium at any point of the SMA wire implies:

$$\sigma(\lambda) = \frac{2T\cdot\sin(\delta\theta/2)}{\delta\lambda} \approx T\cdot\frac{\partial\theta(\lambda)}{\partial\lambda} \quad . \ . \ . \quad \text{(A-1)}$$

Let S_1 be a planar transversal section of the bended structure at curvilinear coordinate λ_1. S_1 crosses the neutral axis of the catheter at a point G_1. The static equilibrium of S_1 is described by:

$$\frac{\delta\boldsymbol{M}(\lambda_1)}{\delta\lambda} + \mathbf{x}_1\times\boldsymbol{N}(\lambda_1) + \boldsymbol{m}(\lambda_1) = 0 \quad . \ . \ . \quad \text{(A-2)}$$

where $\boldsymbol{M}(\lambda_1)$, $\boldsymbol{N}(\lambda_1)$ and $\boldsymbol{m}(\lambda_1)$ are the resulting bending moment, the resulting force and the density of external moment applied to S_1 at G_1, respectively.

Because the stress $\sigma(\lambda)$ is purely radial, $\boldsymbol{m}(\lambda) = 0$ and then:

$$\frac{\delta \boldsymbol{M}(\lambda_1)}{\delta \lambda} = -\mathbf{x}_1 \wedge \boldsymbol{N}(\lambda_1) \quad . \quad . \quad . \quad . \quad . \quad . \quad . \quad . \quad \text{(A-3)}$$

The resulting force $\boldsymbol{N}(\lambda_1)$ at G_1 is obtained by summing the actions of the SMA wire on the catheter for λ ranging from 0 to λ_1:

$$\begin{aligned} \boldsymbol{N}(\lambda_1) &= \boldsymbol{T} + \int_0^{\lambda_1} \boldsymbol{\sigma}(\lambda)\delta\lambda \\ &= -T\mathbf{x}_0 - \int_0^{\lambda_1} T \cdot \frac{\partial \theta(\lambda)}{\partial \lambda}\mathbf{y}_\lambda \delta\lambda \quad . \quad . \quad \text{(A-4)} \end{aligned}$$

By expressing the unit vectors $\mathbf{x}_0$ and $\mathbf{y}_\lambda$ in the base frame attached to the section S_1, Eq. (A-4) becomes:

$$\begin{aligned} \boldsymbol{N}(\lambda_1) &= T \begin{pmatrix} -\cos(\theta_1) \\ \sin(\theta_1) \\ 0 \end{pmatrix} \\ &\quad - \int_0^{\lambda_1} T \left(\frac{\delta\theta(\lambda)}{\delta\lambda}\right) \begin{pmatrix} \sin(\theta_1 - \theta) \\ \cos(\theta_1 - \theta) \\ 0 \end{pmatrix} \delta\lambda \\ \boldsymbol{N}(\lambda_1) &= T \left[\begin{pmatrix} -\cos(\theta_1) \\ \sin(\theta_1) \\ 0 \end{pmatrix} \right. \\ &\quad \left. - \int_0^{\theta_1} \begin{pmatrix} \sin(\theta_1 - \theta) \\ \cos(\theta_1 - \theta) \\ 0 \end{pmatrix} \delta\theta \right] \\ \boldsymbol{N}(\lambda_1) &= T \begin{pmatrix} -1 \\ 0 \\ 0 \end{pmatrix} = -T\mathbf{x}_1 \quad . \quad . \quad . \quad . \quad . \quad . \quad \text{(A-5)} \end{aligned}$$

Finally, Eq. (A-5) into Eq. (A-3) yields:

$$\frac{\delta \boldsymbol{M}(\lambda_1)}{\delta \lambda} = 0 \quad . \quad . \quad . \quad . \quad . \quad . \quad . \quad . \quad . \quad . \quad . \quad . \quad \text{(A-6)}$$

When the catheter is featured with three SMA wires (as the one depicted on **Fig. 3**), the same result can be obtained accounting for the fact that each SMA wire interacts with the catheter the same way as described in **Fig. 12** whatever it is active or passive. In this case, if only one SMA wire is activated while the two others remain passive, the set of axial tip forces applied at the catheter extremity has the configuration shown in **Fig. 14**. Here, T_M stands for the tip force applied by a passive wire and T_A stands for the tip force applied by the active one. Thus, the resulting bending moment applied to section S_0 is:

$$M = r \cdot (T_A - T_M) \quad . \quad . \quad . \quad . \quad . \quad . \quad . \quad . \quad . \quad . \quad . \quad \text{(A-7)}$$

Appendix B.

The tip force T_A is related to the axial strain τ_A undergone by the active SMA wire by:

$$T_A = E_A \tau_A \frac{\pi}{4} d^2 \quad . \quad . \quad . \quad . \quad . \quad . \quad . \quad . \quad . \quad . \quad . \quad \text{(B-1)}$$

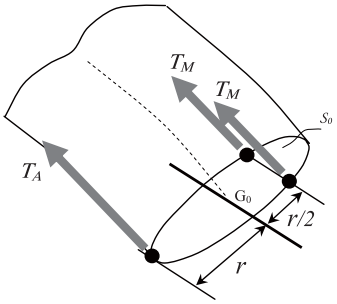

Fig. 14. Tip forces applied to the catheter when one SMA is active and two others are passive.

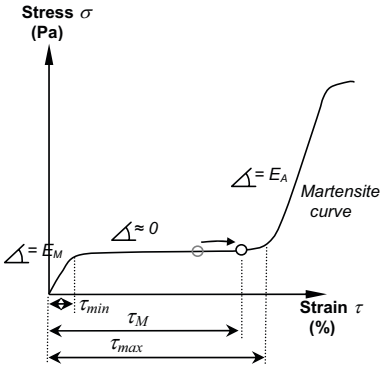

(i) : the functionning point of the two passive wires is such that $\tau_M \leq \tau_{max}$

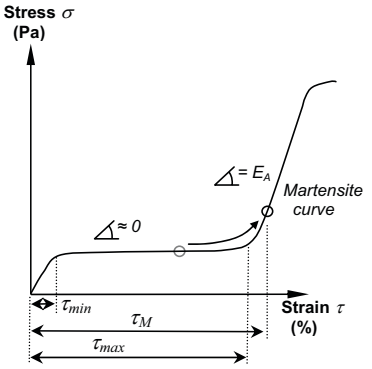

(ii) : the functionning point of the two passive wires is such that $\tau_M \geq \tau_{max}$

Fig. 15. Two cases regarding the location of the functioning point of a passive wire on its martensite curve.

As depicted on **Fig. 15**, the relation between the tip force T_M and the axial strain τ_M undergone by a passive SMA wire depends on the location of the functioning point of this passive wire on its martensite curve:

$$T_M = E_M \tau_{\min} \frac{\pi}{4} d^2 \quad . \quad . \quad . \quad . \quad . \quad . \quad . \quad . \quad . \quad . \quad \text{(B-2)}$$

if $\tau_M \leq \tau_{\max}$ (case (i)) and:

$$T_M = E_M \tau_{\min} \frac{\pi}{4} d^2 + E_A(\tau_M - \tau_{\max}) \frac{\pi}{4} d^2 b \quad . \quad \text{(B-3)}$$

if $\tau_M > \tau_{\max}$ (case (ii)).

Moreover, the strains τ_{init}, τ_A and τ_M are related to the catheter bending angle $\theta_{\max}$ as illustrated in **Fig. 16**. If

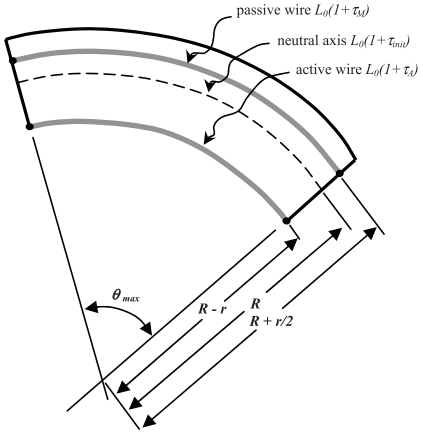

Fig. 16. Relations between the strains undergone by the SMA wires when the catheter is bended and their initial pre-strain.

L_0 is the original length of the SMA wires (no strain), we have:

$$\theta_{\max} = \frac{L_0(1+\tau_{init})}{R} = \frac{L_0(1+\tau_A)}{R-r} = \frac{L_0(1+\tau_M)}{R+{}^{r}/_{2}} \quad \text{(B-4)}$$

and thus:

$$\tau_A = \tau_{init} - \frac{r}{R}(1+\tau_{init})$$

and

$$\tau_M = \tau_{init} + \frac{r}{2R}(1+\tau_{init}) \quad \text{(B-5)}$$

Finally, combining Eq. (A-7) and Eqs. (B-1) to (B-5), the constant bending moment applied to the catheter by the three SMA wires can be rewritten as:

$$M = r \cdot \frac{\pi d^2}{4} \cdot \left[E_A(\tau_{init} - \frac{r}{R}(1+\tau_{init})) - E_M \tau_{\min} \right] \quad \text{(B-6)}$$

in case (i) and:

$$M = r \cdot \frac{\pi d^2}{4} \cdot \left[E_A(\tau_{\max} - \frac{3r}{2R}(1+\tau_{init})) - E_M \tau_{\min} \right] \quad \text{(B-7)}$$

in case (ii).

Besides, this moment is related to the catheter constant radius of curvature

$$R = \frac{\lambda_{\max}}{\theta_{\max}} \text{ by :}$$

$$E_C I_C \frac{\theta_{\max}}{\lambda_{\max}} = M \quad \text{(B-8)}$$

For thin catheters, a current upper bound of the ratio internal radius / external radius is 0.5. In this case, the quadratic momentum I_C can be approximated by:

$$I_C \approx \frac{\pi r^4}{4} \quad \text{(B-9)}$$

At least, if we set $Q = \frac{E_M}{E_A}$ and $K = Q\frac{r^2}{d^2}$, combining Eqs. (B-6) to (B-9) to gives:

$$\theta_{\max} = \frac{\lambda_{\max}}{r}(\tau_{init} - Q\tau_{\min})(K+1+\tau_{init})^{-1} \quad \text{(B-10)}$$

in case (i) and:

$$\theta_{\max} = \frac{\lambda_{\max}}{r}(\tau_{\max} - Q\tau_{\min})\left(K+{}^{3}/_{2}(1+\tau_{init})\right)^{-1} \quad \text{(B-11)}$$

in case (ii).

Appendix C.

For fixed geometrical and physical parameters, the selection between case (i) and case (ii) only relies on the choice of the pre-strain τ_{init} of the wires. The transition value $\hat{\tau}_{init}$ between these two cases can be derived by equalising Eqs. (B-10) and (B-11). It leads to:

$$\hat{\tau}_{init}^2 + b\hat{\tau}_{init} + c = 0 \quad \text{(C-1)}$$

with

$$b = 1 - \frac{2}{3}(\tau_{\max} + \frac{1}{2}Q\tau_{\min} - K)$$

and

$$c = -\frac{2}{3}(\tau_{\max} + \frac{1}{2}Q\tau_{\min} + K)$$

This second order equation has a unique solution regarding the positivity of τ_{init}:

$$\hat{\tau}_{init} = \frac{1}{2}(-b + \sqrt{b^2 - 4c}) \quad \text{(C-2)}$$

which can be closely approximated by:

$$\hat{\tau}_{init} \approx \frac{2K+2}{2K+3}\tau_{\max} \quad \text{(C-3)}$$

by neglecting some second order terms.

Moreover, the partial derivatives of Eqs. (B-10) and (B-11) with respect to the pre-strain τ_{init} are:

$$\frac{\delta\theta_{\max}}{\delta\tau_{init}} = \frac{\lambda_{\max}}{r}\frac{K+1+Q\tau_{\min}}{(K+1+\tau_{init})^2} \quad \text{(C-4)}$$

in case (i) and:

$$\frac{\delta\theta_{\max}}{\delta\tau_{init}} = \frac{\lambda_{\max}}{r}\frac{-{}^{3}/_{2}(\tau_{\max} - Q\tau_{\min})}{\left(K+{}^{3}/_{2}(1+\tau_{init})\right)^2} \quad \text{(C-5)}$$

in case (ii).

The first of these derivatives is always positive while the second one is always negative accounting for the fact that $Q < 1$. Remarking that cases (i) and (ii) correspond to the cases $\tau_{init} \leq \hat{\tau}_{init}$ and $\tau_{init} > \hat{\tau}_{init}$ respectively, proves that $\hat{\tau}_{init}$ constitutes an optimal choice for the SMA wires pre-strain τ_{init} which maximizes the catheter bending angle $\theta_{\max}$.

Name:
Jérôme Szewczyk

Affiliation:
Institut des Systèmes Intelligents et de Robotique (ISIR), Université Pierre et Marie Curie (Paris VI)

Address:
4 Place, Jussieu, Paris 75005, France

Brief Biographical History:
1998- Ph.D. at University of Paris VI
1999- Assistant Professor in Robotics at University of Versailles
1999- Researcher at University of Paris VI

Main Works:
• A. Zahraee, J. Paik, J. Szewczyk, and G. Morel, "Towards the Development of a Hand-Held Surgical Robot for Laparoscopy," IEEE/ASME Trans. on Mechatronics, 2010.
• V. De Sars, S. Haliyo, and J. Szewczyk, "A practical approach to the design and control of active endoscopes," Mechatronics, Elsevier publisher, Vol.20, No.2, pp. 251-264, 2010.
• B. Rosa, P. Mozer, and J. Szewczyk, "An algorithm for calculi segmentation on ureteroscopic images," Int. J. of Computer Assisted Radiology and Surgery, Springer publisher, 2010.

Membership in Academic Societies:
• Institute of Electrical and Electronics Engineers, Inc. (Senior Member IEEE)

Name:
Emilie Marchandise

Affiliation:
Institute of Mechanics, Materials and Civil Engineering, Université Catholique de Louvain (UCL)

Address:
Avenue G., 4 Lemaître, Louvain-La-Neuve 1348, Belgium

Brief Biographical History:
2003- Ph.D. at UCL
2006- Post-Doc in University of Paris Diderot
2008- Assistant Professor in Biomechanics at UCL

Main Works:
• E. Marchandise, J.-F. Remacle, and N. Chevaugeon, "A Quadrature free discontinuous Galerkin method for the level set equation," J. of Computational Physics, Vol.212, No.1, pp. 338-357, 2006.

Membership in Academic Societies:
• European Society of Biomechanics
• Société de Biomécanique

Name:
Patrice Flaud

Affiliation:
Laboratoire Matière et Systèmes Complexes (MSC), Université Paris Diderot

Address:
10 rue A., Domon et L. Duquet, Paris 75013, France

Brief Biographical History:
1988-2000 Head of the Biorheology & Physico-chemical Hydrodynamics Laboratory
1993- Professor at University of Paris Diderot

Main Works:
• "Accurate modelling of unsteady flows in collapsible tubes," Computer methods for Applied Mechanics and Engineering, Vol.13, No.2, pp. 279-290, 2010.
• "Thermal and hydrodynamic modelling of active catheters for interventional radiology," Computer Methods in Biomechanics and Biomedical Engineering, (accepted 2010).
• "An inverse method for non-invasive viscosity measurements," Eur. Phys. J. Appl. Phys., Vol.38, No.79, 2007.

Membership in Academic Societies:
• French Society of Biomechanics
• French Society of Rheology

Name:
Laurent Royon

Affiliation:
Researcher, Laboratoire Matière et Systèmes Complexes (MSC), Université Paris Diderot

Address:
10 rue A., Domon et L. Duquet, Paris 75013, France

Brief Biographical History:
1993- Ph.D. of Physics
2006- Head of Dpt. "Thermal & Energy Engineering," Marne la Vallée University

Main Works:
• "Thermal and hydrodynamic modelling of active catheter for the neuroradiology," Computer Methods in Biomechanics and Biomedical Engineering, (accepted 2010).
• "Flow investigation of phase change material (PCM) slurry as a heat transfer fluid in a closed loop system," Int. J. Energy Research, Vol.33, No.4, pp. 333-341, 2009.
• "Forced convection heat transfer in a slurry of phase change material in an agitated tank," Int. Comm.. Heat & Mass transfer, Vol.27, No.6, pp. 1057-1065, 2000.

Membership in Academic Societies:
• The French Society of Energetic
• The French Society of Rheology

Name:
Raphaël Blanc

Affiliation:
Bichat School of Medicine and Department of Functional and Interventional Neuroradiology, Fondation Rothschild Hospital, University of Paris VII

Address:
25-29 rue Manin, Paris 75940, France

Brief Biographical History:
1998-2003 Medical Doctor, Faculty of Medicine, University of Bourgogne
2003-2008 Fellowship, Interventional Neuroradiology, Henri Mondor Hospital, Créteil
2008- Department of Functional and Interventional Neuroradiology, Fondation Rothschild Hospital

Main Works:
• M. Piotin, R. Blanc, L. Spelle, C. Mounayer, R. Piantino, P. J. Schmidt, and J. Moret, "Stent-assisted coiling of intracranial aneurysms," clinical and angiographic results in 216 consecutive aneurysms, Stroke, Jan, Vol.41, No.1, pp. 110-115. Dec 3, 2010.
• C. Lin, R. Blanc, F. Clarencon, M. Piotin, L. Spelle, J. Guillermic, and J. Moret, "Overlying Fluoroscopy and Preacquired CT Angiography for Road-Mapping in Cerebral Angiography," AJNR American J. of Neuroradiology, Vol.31, No.3, pp. 494-495, 2010.
• R. Blanc, A. D. Maia Barros, P. Brugieres, J. F. Meder, and A. Gaston, "Cavernous sinus dural arteriovenous fistula complicated by edematous cerebral lesions from venous etiology," J. of Neuroradiology, Vol.31, No.3, pp. 220-224, 2004.
• R. Blanc, C. Mounayer, M. Piotin, J. C. Sadik, L. Spelle, and J. Moret, "Hemostatic closure device after carotid puncture for stenting and coiling of an intracranial aneurysm : immediate and long term follow up," AJNR American J. of Neuroradiology, Vol.23, pp. 978-981, 2002.

Membership in Academic Societies:
• French Society of Radiology
• French Society of Neuroradiology
• World federation of therapeutic interventional neuroradiology